Journal of Applied Physics

Study of exciton-polaron interaction in pentacene field effect transistors using high sensitive photocurrent measurements

Cite as: J. Appl. Phys. **126**, 145501 (2019); https://doi.org/10.1063/1.5116412
Submitted: 25 June 2019 . Accepted: 22 September 2019 . Published Online: 09 October 2019

Haripriya Kesavan, Subhamoy Sahoo, Sanjoy Jena, Prashanth Kumar Manda, Amogh Kumar Baranwal, Soumya Dutta, Jayeeta Bhattacharyya, and Debdutta Ray

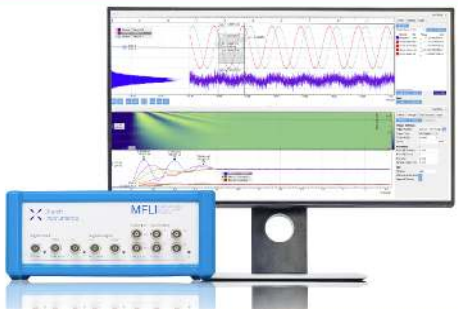

Journal of Applied Physics ARTICLE scitation.org/journal/jap

Study of exciton-polaron interaction in pentacene field effect transistors using high sensitive photocurrent measurements

Cite as: J. Appl. Phys. **126**, 145501 (2019); doi: 10.1063/1.5116412
Submitted: 25 June 2019 · Accepted: 22 September 2019 ·
Published Online: 9 October 2019

Haripriya Kesavan,[1,a)] Subhamoy Sahoo,[2] Sanjoy Jena,[1] Prashanth Kumar Manda,[1] Amogh Kumar Baranwal,[1] Soumya Dutta,[1] Jayeeta Bhattacharyya,[2] and Debdutta Ray[1,b)]

AFFILIATIONS

[1]Department of Electrical Engineering, Indian Institute of Technology Madras, Chennai 600036, India
[2]Department of Physics, Indian Institute of Technology Madras, Chennai 600036, India

[a)]**Electronic mail:** ee14d021@ee.iitm.ac.in
[b)]**Electronic mail:** dray@ee.iitm.ac.in

ABSTRACT

Luminescence quenching in the presence of polarons is one of the major challenges in organic light emitting devices. In this work, exciton quenching in the presence of polarons is studied using phase sensitive photocurrent measurements on pentacene field effect transistors. The enhancement of conduction in the organic field effect transistors on light illumination is studied using photocurrent spectral response measurements and corresponding optical simulations. The photocurrent is shown to be governed by the polaron mobility and the exciton quenching efficiency, both of which depend on the polaron density in the channel. Two models are proposed on the exciton dynamics in the presence of gate induced polarons in the transistor channel. The first model simulates the steady-state exciton concentration profile in the presence of exciton-polaron interaction. The second one is a three-dimensional steady state exciton-polaron interaction model, which supports the findings from the first model. It is shown that the excitons quench by transferring its energy to polarons, thereby promoting the latter to high energy states in the density of states manifold. The polarons move in the higher energy states with greater microscopic mobility before thermalizing, thereby leading to an enhancement of conduction. It is observed that for the present system, where charge carrier transport is by hopping, all polarons interact with excitons. This implies that for low mobility systems, the interaction is not limited to deep trapped polarons.

I. INTRODUCTION

Optoelectronic devices using organic semiconductors have gained significant attention.[1–3] Strong exciton binding energy in these materials make radiative recombination efficient, and organic light emitting diodes (OLEDs) with a 100% internal quantum efficiency have been reported.[4–6] The first organic laser diode (OLD) is recently shown,[7] which opens up new possibilities of cheap and compact laser technology. However, the development of an efficient OLD face various challenges: (1) difficulty in achieving a high current density for population inversion due to the inherent low mobility of organic materials,[8,9] (2) quantum efficiency roll-off at high current densities because of various exciton loss processes such as field induced exciton dissociation,[10–12] metal contact induced exciton quenching,[13,14] exciton-exciton interaction,[15–17] triplet absorption,[7,18] and exciton-polaron interaction (EPI).[19–23]

Organic light emitting transistors (OLETs) are promising candidates for electrically pumped organic semiconductor lasers owing to their high channel mobility and reduced exciton losses compared to OLEDs.[9,24,25] The major luminescence quenching mechanism in OLETs is EPI, due to the high polaron density present in the channel region.[24–26] EPI in organic semiconductor devices has been studied using diode[27–29] as well as transistor[24,26,30] structures. Since multiple exciton quenching processes coexist in diodes, decoupling the effect of EPI is a challenge. The field-effect transistor (FET) structure gives a better platform for this study due to the following reasons: (i) negligible electric field-induced exciton dissociation in

FETs as the lateral (drain-source) electric field is too low to cause any significant exciton dissociation, and the vertical (gate-source/drain) electric field is screened by polarons in the channel at the semiconductor/insulator (S/I) interface,[24,26,30] (ii) negligible exciton quenching at the metal (source/drain) electrodes for a long channel FET with uniform exciton generation in the channel, (iii) the high polaron density in the channel provides an efficient interaction zone for excitons and polarons, and (iv) the gate control allows the study of EPI for different polaron densities.

Polaron-induced exciton quenching in the channel region of organic FETs (OFETs) was reported earlier, where the photoluminescence (PL) quenching was measured as a function of the applied gate-to-source voltage (V_{GS}).[24,26,30] Hansen *et al.*[26] suggested that the quenching may be due to excitons interacting with carriers residing in the deep trap states. From transient photoluminescence (PL) measurements, Koopman *et al.*[24] proposed the role of all polarons in EPI. In this work, phase-sensitive photocurrent is used as the probe to study EPI in an OFET structure. The material chosen for this study is pentacene due to its relatively high hole mobility,[31,32] high absorption in the visible spectrum,[33] and that OFETs with greatly reduced nonidealities can be fabricated.[31,32,34]

The charge carrier dynamics as a result of the quenching of excitons by EPI is studied. Charge carrier transport in polycrystalline systems such as the one studied in this work is by hopping along the density of states (DOS) manifold.[35] The charges are polaronic in nature. The hopping is by a combination of thermal activation and tunneling. The localization of the polaron depends on its position in the DOS manifold. The contribution of the polarons, residing in various levels of localization, to EPI is investigated.

II. EXPERIMENTAL SECTION

A. Device fabrication

Pentacene FETs are fabricated in the bottom-gate bottom-contact geometry. Thermally grown SiO_2 (65 nm) on an n^+ silicon wafer is used as the gate insulator and the other side of wafer as the bottom gate. Metallization for the source/drain contact is carried out by a controlled deposition of chromium (2.5 nm)/palladium (25 nm) on SiO_2 at 0.5 Å/s with electron beam evaporation. Source/drain patterning is performed by photolithography (lift-off). The samples are then treated with Octa Decyl Trichloro Silane (ODTS) followed by annealing at 150 °C for 2 h. This process reduces the Silanol (Si-OH) groups at the SiO_2 interface, which otherwise act as interface trap centers.[36] This ensures very low trap density at the S/I interface. Pentacene (triple sublimed grade, 99.995%) is deposited at 0.7 Å/s at room temperature, using thermal evaporation under a base pressure of 10^{-7} mbar. All the devices used in this study are from the substrates processed in the same batch and from the same SiO_2 wafer, but the surface treatment and pentacene deposition are performed at different times, assuring the same conditions throughout. Devices with a 60 μm channel length (L) and a 0.6 mm channel width (W) are used for measurements.

B. Electrical characterization

All electrical characterizations of the transistors under dark and lighted conditions are carried out in a vacuum probe station with a base pressure less than 10^{-5} mbar (PLV50, SussMicroTec GmbH) to avoid device degradation. An Agilent B1500A parameter analyzer is used for all direct current (DC) measurements. The block diagram of the experimental setup used for the photocurrent measurements is given in the supplementary material (Fig. S1). Light from the monochromator source is chopped at a low frequency (~130 Hz) and is coupled to the probe station by using a fiber optic light guide. Light spot coupled to the probe station has a diameter of 0.5–0.6 mm. The chopper provides a reference electrical signal of the chopping frequency, which is fed as an input to the lock-in amplifier. Gate and drain biases of the transistor are sourced from the parameter analyzer. The source-to-drain current of the transistor, which consist of a DC component due to field induced polarons, and the chopped photocurrent, is provided as an input to the lock-in amplifier through a preamplifier. The preamplifier is a high-gain current-to-voltage converter with a gain ranging from 10^3 to 10^8 V/A. For external quantum efficiency (EQE) measurements, photocurrent spectrum is normalized with a calibrated silicon photodetector response. The photocurrent-voltage measurements are carried out with a white light source (using a Xenon lamp).

III. RESULTS AND DISCUSSIONS

A. Pentacene field-effect transistor as a tool for the study

Figure 1 shows the measured output and transfer characteristics of the bottom-gate bottom-contact OFET used for this study. The basic structure of the fabricated OFET is shown in the inset of Fig. 1(b). The output characteristics show negligible schottky contact resistance, due to the alignment of the palladium work function with the highest occupied molecular orbital (HOMO) of pentacene, therefore, ensuring sufficient charge accumulation in the channel for excitons to interact with. The transfer characteristics show very low hysteresis and nearly zero switch on voltage (V_{sw}), which implies that deep level trap density is negligible in these devices.

The Sentaurus TCAD[37] simulations of electric field (E) and polaron density (p) for the OFET with a pentacene thickness of 50 nm and an oxide thickness of 65 nm, with an applied drain and gate bias of −10 V, are shown in Fig. 2. The electric field at the pentacene-SiO_2 interface in the middle of the channel is 1.3×10^6 V/cm and it drops down to 2.9×10^5 V/cm within one monolayer (1.5 nm) from the interface. According to earlier reports, a high electric field in the order of 10^6 V/cm can contribute to exciton dissociation in pristine organic devices; however the reported values of dissociation efficiency are in the order of 0.1–10%.[38–40] As the electric field reduces nonlinearly toward the bulk, the field-induced exciton dissociation becomes negligible in subsequent monolayers from the interface.

It can be noted from Fig. 2(b) that the high polaron density near the interface drops down by one order of magnitude within one monolayer of pentacene. Hence, the accumulation layer thickness can be approximated as one monolayer from the S/I interface and the EPI is expected to occur dominantly near the interface. The variation of polaron density profile with gate voltage and film thickness is given in Fig. S2 of the supplementary material.

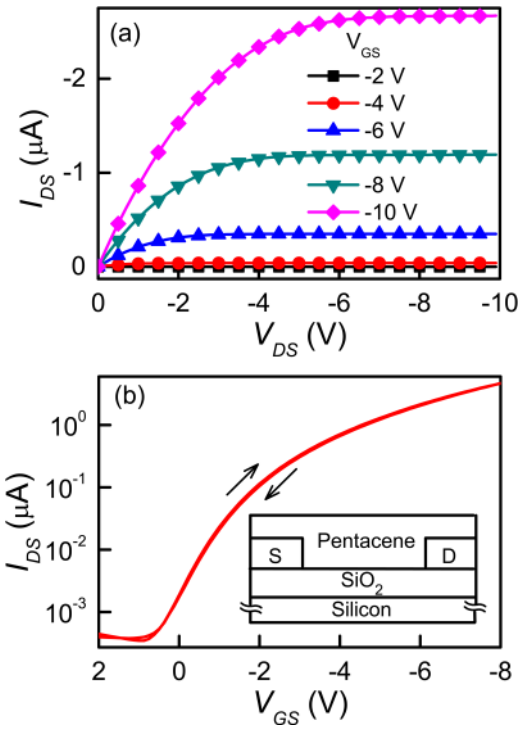

FIG. 1. Measured (a) output characteristics [drain-to-source current (I_{DS}) vs drain-to-source voltage (V_{DS})] of a pentacene FET with a channel length (L) and width (W) of 60 μm and 6000 μm, respectively. (b) Transfer characteristics [drain-to-source current (I_{DS}) vs gate-to-source voltage (V_{GS})] of a pentacene FET at $V_{DS} = -10$ V. The schematic of the fabricated device in the bottom-gate bottom-contact geometry is shown in the inset.

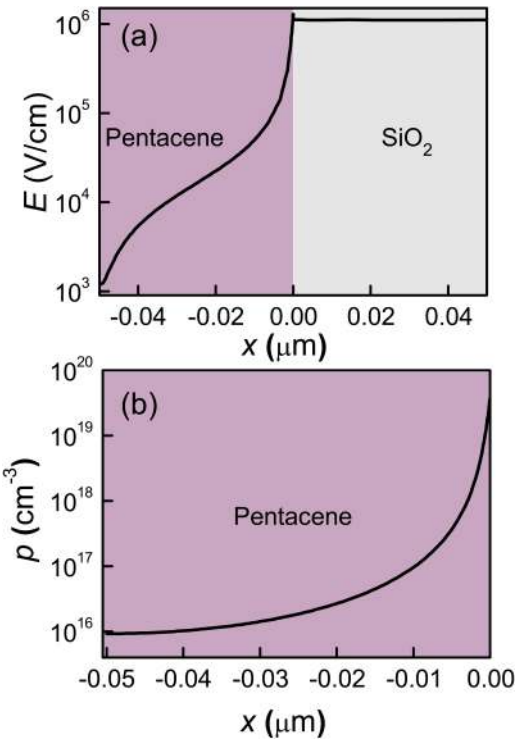

FIG. 2. Sentaurus TCAD simulation of (a) electric field (E) and (b) polaron density (p) for the OFET with a pentacene thickness of 50 nm and an oxide thickness of 65 nm, with an applied drain and a gate bias of −10 V. Variations along the thickness (x-direction) in the middle of the channel are shown.

B. External quantum efficiency: Measurements and simulations

The major photocarrier generation process is identified by photocurrent spectral response measurements. A sensitive measurement technique through a high gain lock-in amplifier is used as explained in Sec. II. The device is uniformly illuminated with monochromatic light from the top of the pentacene layer. The EQE of the transistor is obtained from the measured photocurrent as a function of illumination wavelength. The EQE for different bias conditions is given in Sec. 3 of the supplementary material. One can note that the EQE spectral shape is independent of both gate and drain voltages for the voltage ranges shown.

Figure 3(a) compares the EQE spectrum of an OFET with the bulk absorption spectrum of a pentacene film (experimentally measured and simulated) for a pentacene layer thickness of 50 nm. All spectra are normalized to the corresponding values at 660 nm peak. The experimental absorption spectrum is measured for pentacene on the glass substrate. The simulated absorption spectrum of pentacene (on the SiO_2-silicon substrate) is obtained from the transfer matrix method (TMM) simulation[41] using the optical constants obtained from spectroscopic ellipsometer measurements (Fig. S4 in the supplementary material). This simulation accounts for the optical interference effects in pentacene due to the multilayer structure. It is observed that while the peak positions are unchanged, the EQE does not follow the absorption spectrum. In the EQE spectrum, the relative contribution of peaks/shoulders at 545 nm, 580 nm, and 630 nm is higher compared to that in the absorption spectrum. If all excitons generated in the pentacene film contribute to photocurrent with the same probability, then bulk absorption spectrum and EQE spectrum will have the same shape. Since the charge carrier transport is wavelength independent, the observed change in the EQE spectrum must arise from a wavelength dependent photocarrier generation process.

In order to understand the possible reasons for this observation, transistors with five different pentacene layer thicknesses ranging from 25 nm to 200 nm are fabricated and their EQE spectra are compared in Fig. 3(b). As the thickness increases, the highest peak of the EQE spectra gets suppressed. The relative peak strength changes with increasing thickness till 100 nm, after which there is no visible variation in the spectral shape of EQE.

A reason for this observation can be that the photogeneration occurs dominantly near the S/I interface. For wavelengths where the absorption coefficient (α) is high, the majority of the absorption takes place near the top surface (far from the S/I interface) compared to the wavelengths where α is low. Therefore, the chance of excitons recombining before reaching the S/I interface is more.

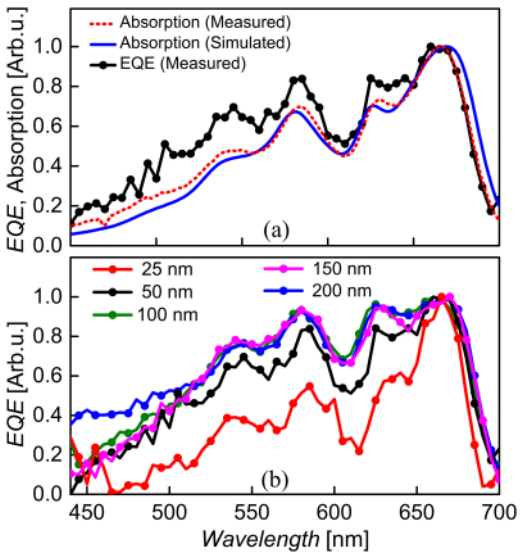

FIG. 3. (a) Comparison of the EQE spectrum of a pentacene FET and the bulk absorption spectrum of a pentacene film (experimentally measured and simulated) for a pentacene layer thickness of 50 nm. All spectra are normalized to the 660 nm peak. (b) Normalized EQE spectra (measured) of OFETs with pentacene thicknesses ranging from 25 nm to 200 nm. EQE measurements are taken for $V_{GS} = -10$ V and $V_{DS} = -10$ V. The film thickness was measured using a spectroscopic ellipsometer as well as with an optical profilometer. Both the methods yielded the same film thickness within $\pm$10% error.

This implies that the fraction of excitons contributing to photocurrent at the S/I interface can be larger for wavelengths where α is low. The wavelength-screening effect[42] as discussed above will be more pronounced for devices with thicker films as a smaller fraction of bulk-generated excitons can reach the S/I interface. It is also observed that for pentacene thickness of more than 100 nm, the spectral response does not show any visible shift in relative peak intensities. The reason can be that for higher pentacene thicknesses, the contribution of bulk photogeneration becomes significant and reduces the effect of interface photocurrent on the EQE spectrum.

In order to study the relative contribution of interface and bulk photogeneration processes to the photocurrent, the EQE is simulated from the absorption spectra for the pentacene-SiO_2-silicon structure using TMM. The TMM simulation quantifies the exciton generation rate from the optical field, as a function of wavelength and depth in the pentacene layer. Here, the assumption is that only one type of exciton takes part in the photocarrier generation process and, therefore, the wavelength dependence of EQE can be explained by the absorption alone. Here, we consider two possibilities for the photogeneration of charge carriers: a V_{GS}-dependent process occurring near the S/I interface and V_{GS}-independent processes in the film, such as spontaneous generation of free charge carriers[43] or dissociation of excitons at traps/defects,[39] which is the dominant process in the bulk region. This is a reasonable assumption in the presence of the rapidly reducing gate effect from the S/I interface to the bulk, as discussed in Fig. 2.

Figure 4(a) shows the structure used for TMM simulations. The active layer thickness (L_a) is the sum of the transistor accumulation layer thickness ($\sim$1.5 nm), the exciton-polaron interaction distance ($R_c \sim 2$ nm), i.e., the separation between an exciton and a polaron within which the interaction will take place[24,44] and the exciton diffusion length (L_{ex}). It is assumed that all excitons which are generated within the active layer can diffuse to the S/I interface and contribute to the photocurrent with a certain probability. The rest of the pentacene layer is treated as the bulk, where the excitons recombine before they can reach the interface. The whole photocarrier generation processes in the bulk is assigned with a constant probability.

The EQE as a function of the incident wavelength is simulated from the weighted absorption of the active layer and the bulk, by considering two different photocarrier generation probabilities for these regions. Hence, the simulated (EQE_{simul}) can be written as

$$\begin{aligned} EQE_{simul} &= Abs_a \times p_a + Abs_b \times p_b \\ &= p_a(Abs_a + Abs_b \times f) \quad f = \frac{p_b}{p_a}, \end{aligned} \tag{1}$$

where p_a (p_b) and Abs_a (Abs_b) are the active layer (bulk) photocarrier generation probability and absorption, respectively. Abs_a and Abs_b are obtained by integrating the exciton generation rate in the corresponding regions and f is the relative photocarrier generation efficiency of bulk with respect to the interface.

The normalized EQE_{simul} spectrum is compared with the normalized experimental EQE (EQE_{exp}) spectrum with f and L_a as fitting parameters, for devices with five different pentacene thicknesses. The results are shown in Figs. 4(b)–4(f). The normalized absorption spectra of the entire pentacene film are also shown for the reference. It can be noted that the mismatch in the EQE spectrum with the total absorption spectrum is higher for thicker films. The experimental EQE resembles the simulated EQE for $L_a = 10 \pm 2$ nm and $f = 3 \pm 2$%, for all the devices. A small value of f implies that the photocarrier generation efficiency in the bulk is around 3% of that in the active layer. Since we are extracting the parameters from normalized plots, invariance of spectral shape with V_{GS} implies invariance of the values of fitting parameters with V_{GS}. Independence of the fitting parameters on film thickness and bias conditions shows the robustness of our simulation study and reliability of the values of the extracted fitting parameters.

The analysis proves that a highly efficient photocarrier generation process exists near the S/I interface (accumulation region). Any mismatch in the spectral shape of EQE_{exp} and EQE_{simul} can arise from: (i) existence of more than one type of exciton species which can lead to wavelength-dependent changes in the photocurrent, (ii) any deviation from the actual optical constants of pentacene film, to that obtained from ellipsometer fittings, especially for wavelengths where the absorption coefficient is low.

Triplet exciton generation from singlet fission has been observed in pentacene.[45,46] However, an exciton diffusion length of $\sim 6.5 \pm 2$ nm (obtained from L_a) shows that triplet states do not contribute to the interface photocurrent, as the reported exciton diffusion length of triplets in the polycrystalline pentacene is in the

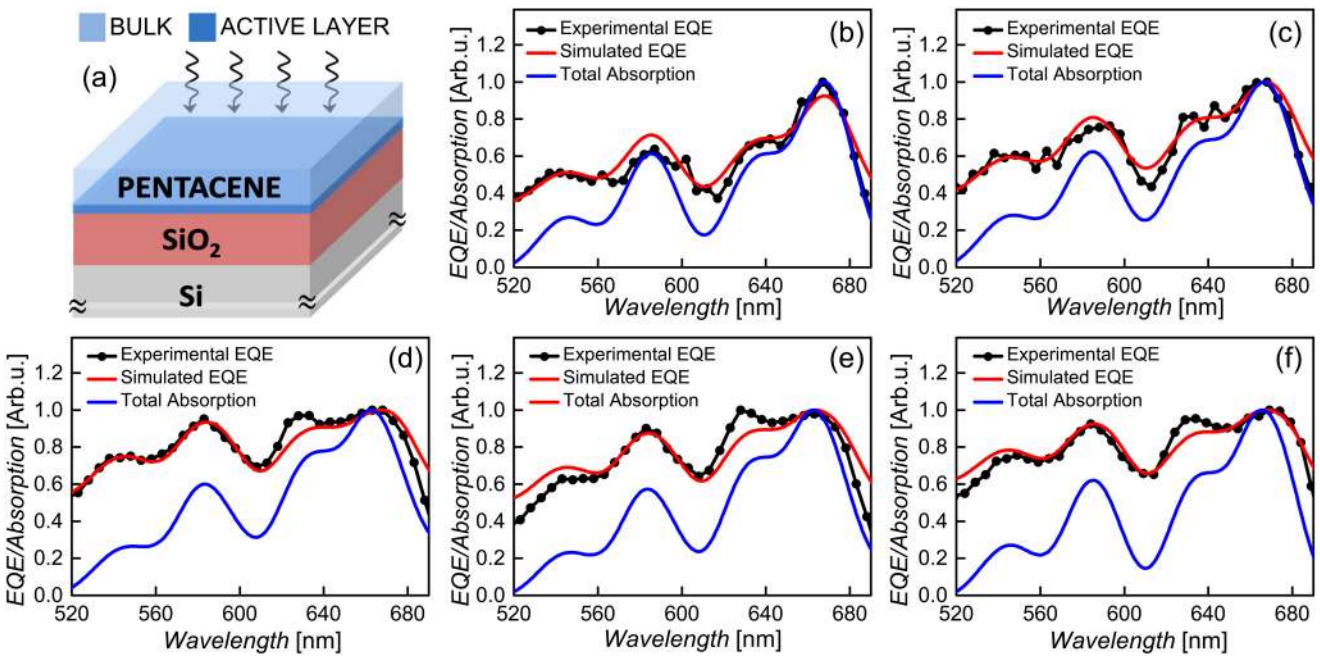

FIG. 4. (a) Silicon/SiO_2/pentacene structure used for the transfer matrix method (TMM) simulation. The SiO_2 thickness is 65 nm. The active layer in pentacene, within which the generated excitons can diffuse to the interface, is shown as dark blue. The bulk region shown as light blue is where excitons recombine before reaching the interface. (b)–(f) Normalized plots of experimental EQE spectra of OFETs (black lines with dots), corresponding simulated EQE spectra obtained from the TMM simulation (red lines) and the total absorption taking place in the full thickness of the film (obtained from TMM simulation, blue lines) for pentacene film thicknesses of 25 nm, 50 nm, 100 nm, 150 nm, and 200 nm, respectively. The active layer thickness (L_a) is obtained as 10 ± 2 nm, and the bulk contribution to EQE relative to the active layer contribution (f) is found to be 1%–5% for all the devices. All EQE measurements are taken for $V_{GS} = -10$ V and $V_{DS} = -10$ V. The EQE spectral shape does not vary with applied voltages for the voltage ranges used.

range of 40–80 nm.[47,48] If triplets are contributing to photocurrent, the extracted L_{ex} must be in the range of the triplet exciton diffusion length. Therefore, the observed pathway of the photocarrier generation is dominantly from singlets or singlets with an excimer character.[49]

C. Gate bias modulation of photocarrier generation

Section III B showed the presence of efficient photocarrier generation near the S/I interface of OFET. In order to understand the mechanism of this process, the variation of the photogenerated polaron concentration (n_{PH}) as a function of V_{GS} needs to be studied. In the linear region of transistor operation, the photocurrent (I_{PH}) depends on n_{PH} and channel mobility (μ) as $I_{PH} = W\mu n_{PH} V_{DS}/L$, where V_{DS} is the applied drain-to-source voltage. The channel mobility in OFET is a function of V_{GS}. The DOS in these systems can be modeled as a manifold of localized states, where the charge carrier motion is dominated by hopping.[35,50] Populating the DOS will lead the carriers to access states with lower interstate separation and higher tunneling probability, which leads to an increase in the mobility with V_{GS}.[35] Therefore, V_{GS}-dependence of photocurrent is due to both n_{PH} and μ. The DOS illustration is given in Sec. III D (Fig. 8).

Photocurrent in the linear region of the OFET and the experimentally measured mobility with its linear fit, as a function of V_{GS}, are shown in Figs. 5(a) and 5(b), respectively. The determination of mobility from the transfer characteristics, as usually done for inorganic material based transistors, is the common practice in OFETs.[51] However, this method is correct only when the mobility is independent of V_{GS}.[52] Due to its V_{GS}-dependence, the mobility is extracted from the triode region of the I_{DS} vs V_{DS} plot, for different values of V_{GS}. Extraction of mobility from the triode region avoids the effect of contact resistance in the mobility values. Mobility is found out from the slope of the output conductance ($g_{DS} = \frac{\partial I_{DS}}{\partial V_{DS}}$), in the region where g_{DS} varies linearly with V_{GS} (i.e., triode region). The error bars shown in the mobility plot [Fig. 5(b)] correspond to the variation over multiple devices.

From the I_{PH} vs V_{GS} and μ vs V_{GS} plots, the functional form of n_{PH} with V_{GS} can be estimated [n_{PH} is given as $I_{PH}L/(W\mu V_{DS})$]. The photogenerated polarons do not cause a significant change in μ as the intensity of light used for the measurement is low. This allows for the decoupling of n_{PH} and μ.

Figure 6 shows the comparison of the gate bias dependence of photocurrent and the mobility in the linear-regime (plots are normalized at $V_{GS} = -10$ V). Photocurrent is measured for devices of different semiconductor thicknesses. n_{PH} is extracted from I_{PH} and

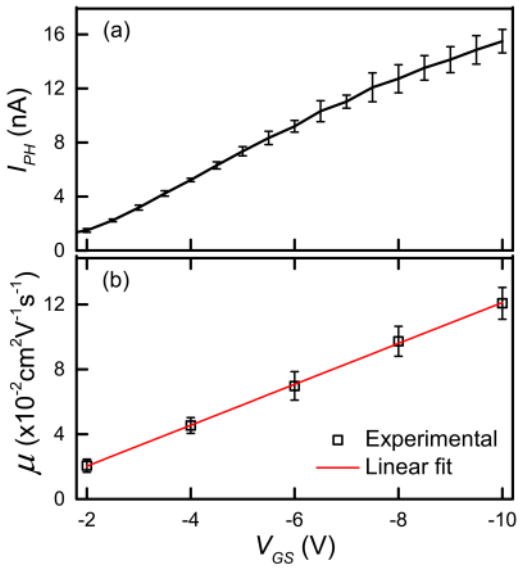

FIG. 5. (a) Photocurrent (I_{PH}) variation with gate-to-source voltage (V_{GS}) for a pentacene FET at a drain-to-source voltage (V_{DS}) of −1 V. Photocurrent measurements are carried out with a white light source (using a Xenon lamp). (b) Channel mobility (μ) variation with V_{GS} extracted from the triode region of the I_{DS}–V_{DS} plot (symbols) and the linear fit to mobility (solid line) with a root mean square error of 0.1%.

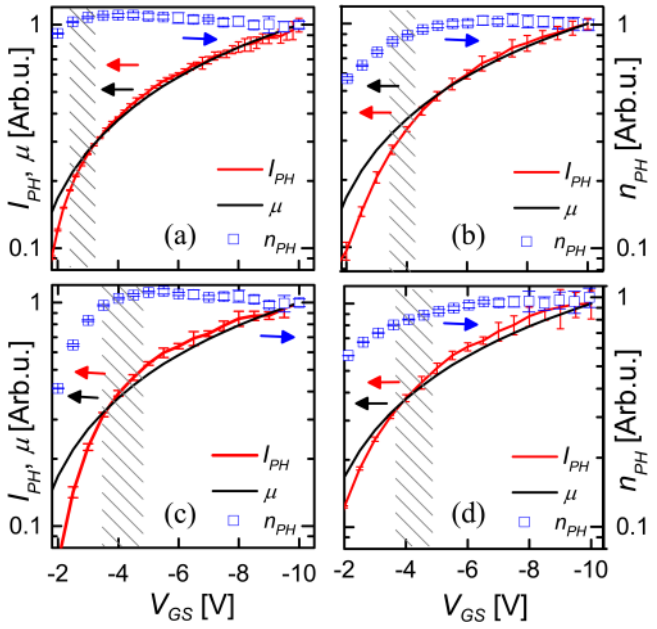

FIG. 6. Channel mobility (μ), photocurrent (I_{PH}), and effective photocarrier concentration (n_{PH}), all normalized to their corresponding values at $V_{GS} = -10$ V, plotted as a function of V_{GS} (in a semilogarithmic graph), for OFETs with pentacene thicknesses of (a) 50 nm, (b) 100 nm, (c) 150 nm, and (d) 200 nm. The left-hand Y axis is I_{PH} and μ, and the right-hand Y axis is n_{PH}, for all the figures. I_{PH} measurements are taken at $V_{DS} = -1$ V. The shaded area corresponds to the knee region, where n_{PH} saturates.

from the linear fit of μ. Figure 6 shows n_{PH} normalized to its value at $V_{GS} = -10$ V. The plots are shown from $V_{GS} = -2$ V in order to restrict the measurements to the linear region of transistor operation ($V_{sw} \sim 0$ V for all the devices). Therefore, the n_{PH} plot does not include the full variation. However, Fig. 6 clearly shows the knee region where n_{PH} saturates. The mobility and photocurrent match well for $|V_{GS}| \gtrsim 4 \pm 1$ V. This implies that in this voltage range, the photogeneration of polarons is independent of V_{GS} and, therefore, the photocurrent variation is due to mobility variation alone. However, when V_{GS} is lowered, photocurrent starts deviating from mobility and shows higher V_{GS} dependence compared to mobility. This means that photocarrier generation varies with V_{GS} at low V_{GS}. An increase in n_{PH} followed by saturation with a knee at V_{GS} of around -4 ± 1 V can be observed from these plots. The shaded area in the figure represents the knee where n_{PH} starts to saturate.

Jia *et al.* hypothesized that n_{PH} is independent of V_{GS},[53] and the polarons were found to be formed by exciton dissociation at oxygen-mediated traps at the S/I interface. However, this work observes a clear increase in n_{PH} up to $|V_{GS}| \simeq 4 \pm 1$ V, followed by a saturation. Moreover, the surface passivation technique (explained in Sec. II) ensures a low trap density at the S/I interface. This is confirmed from the nearly zero V_{sw} and low hysteresis in the transfer characteristics [Fig. 1(b)]. The trap density estimated from the subthreshold swing[52] in the devices reported here is in the range of 10^{17} cm^{-3}. A gate voltage less than −0.3 V is sufficient to fill these trap levels. This can be observed from the simulation of the polaron density profile [Fig. S2(a)], where the injected polaron density in the device is above 10^{17} cm^{-3} for $|V_{GS}| > 0.2$ V. Thus, if only deep level traps are responsible for the observed photocarrier generation, the n_{PH} must saturate at very low V_{GS} ($|V_{GS}| \lesssim 0.3$ V).

Lloyd-Hughes *et al.* reported electric field-assisted exciton dissociation in the polymer FET, where the dissociation efficiency was found to be ∼0.1 at an electric field of ∼10^6 V/cm.[40] However in the device reported here, photocarrier generation tends to saturate around $V_{GS} = -4$ V, which corresponds to an average electric field of around 6×10^5 V/cm at the S/I interface. This field is not large enough to dissociate all the excitons reaching the S/I interface[39,43] as the existing models for electric field assisted dissociation of the Frenkel exciton suggests a gradual increase in the probability of dissociation with the field, reaching a significant value of dissociation efficiency above 10^6 V/cm.[54,55] Hence, field dependent exciton dissociation is not a reason for the observed n_{PH} saturation with V_{GS}.

EPI can result in V_{GS}-dependent exciton quenching in the accumulation region of OFET. An increase in PL quenching at a low V_{GS} followed by saturation above a V_{sw} was observed in OFETs with pristine organic small molecules, which was attributed to EPI near the S/I interface.[24,26,30] Since photogeneration in the present study and PL quenching show similar trends with gate voltage, it can be presumed that the mechanism behind both the observations is probably the same.

D. Gate voltage modulation of exciton density

1. Simulation of steady-state exciton concentration

In this section, the exciton dynamics under the influence of injected polaron distribution is modeled, which gives insights into the origin of the observed characteristics of photocarrier generation. The steady-state exciton concentration (n_{ex}) as a function of depth (x), wavelength (λ), and V_{GS} is obtained by solving the exciton transport and continuity equations in the presence of EPI, similar to what was reported in earlier studies.[24] The exciton generation rate in a pentacene layer is determined by the TMM simulation (explained in Sec. III B), and the polaron density profile is obtained from Sentaurus TCAD simulations (Fig. S2). The details of the simulation of exciton dynamics are explained in the supplementary material (Sec. 5).

Using n_{ex} obtained from the simulation (Fig. S5 in the supplementary material), the relative exciton quenching (η), defined as the change in the steady state exciton concentration with V_{GS} compared to $V_{GS} = 0$ V case, is calculated as

$$\eta(V_{GS}) = \frac{N_{ex}(0) - N_{ex}(V_{GS})}{N_{ex}(0)}, \tag{2}$$

where $N_{ex}(V_{GS})$ corresponds to the total number of excitons (n_{ex} integrated over x and λ) for a given V_{GS}. η indicates how the total number of steady-state excitons in the device is modulated by the gate voltage and thereby EPI rate (EPI being the only V_{GS}-dependent quenching process). Qualitatively, η resembles the photoluminescence electro-modulation (PLEM).[24]

Figure 7(a) shows the variation of η with V_{GS} for different pentacene thicknesses. One can note that η decreases with an increase in the pentacene thickness, which can be understood in the following way. From Fig. S2(b) of the supplementary material, it can be noted that the polaron density profile (hence the EPI rate) near the S/I interface does not change with the pentacene film thickness. This means that for a larger pentacene thickness, a smaller fraction of excitons will diffuse to the polarons and get quenched; hence, η reduces with an increase in the thickness. A similar trend is observed for variations of PLEM with semiconductor thickness.[30] Figure 7(b) shows η for different pentacene thicknesses normalized to the respective values at $V_{GS} = -10$ V. η tends to saturate at around $V_{GS} \sim -4$ V, which is around the voltage at which n_{PH} saturates ($V_{GS} = -4 \pm 1$ V). The observed similarity in the saturation trend for η and n_{PH} means that the same phenomena govern both of the quantities, that is, EPI.

The observed photocarrier generation can be interpreted by the activation of localized charge carriers by the energy transfer through EPI. It is known that exciton quenches near a polaron by transferring its energy through the Forster resonant energy transfer (FRET).[20,22,29,56] As a result, the polaron get excited to the higher energy states in the DOS manifold and eventually thermalizes back to the initial state.[23,57] Menke *et al.* showed that photons of energy 0.9 eV can lead to the dissociation of charge transfer (CT) excitons, resulting in the activation of polarons to higher delocalized states.[58] Frenkel excitons, upon quenching, can cause a similar activation.[23,57] It is to be noted that the polarons in the channel are at a higher state of delocalization compared to bound CT states. Since the channel mobility [Fig. 5(b)] is roughly two orders of magnitude smaller than that of the crystalline pentacene,[59] it can be inferred that charge transport occurs by hopping through localized states.[35] On illumination, the generated excitons diffuse toward the S/I interface and quench at the polaron sites, thereby promoting the polarons to higher energy states where they can travel with a higher mobility. This process is shown in Fig. 8. A Gaussian DOS is assumed with a width of 100 meV, which is close to the reported values for pentacene.[36] In the high energy states of the DOS, polarons experience a higher microscopic mobility[60] due to the reduced tunneling barrier and thereby an increased hopping rate.[35] The higher energy states are more delocalized compared to lower energy states. If the average hopping time in the higher energy state is less than the thermalization time of the activated polaron, the polaron can move in the higher energy states with a greater microscopic mobility under the influence of the applied electric field (due to V_{DS}). This results in an increase in the total device current, and a nonzero photocurrent is detected by the lock-in amplifier. Photomultiplication in organic materials due to EPI has been reported earlier, where charge carrier equilibration time is theorized to be much higher than the transit time over the device length.[57] The results reported here support such an observation, where the activated polaron moves in a "hot" state before thermalization.

The activation of polarons to high mobility states which results in photocurrent can be viewed as an effective increase in the number density of delocalized polarons under illumination. This is the extracted n_{PH} from the photocurrent and mobility as shown in

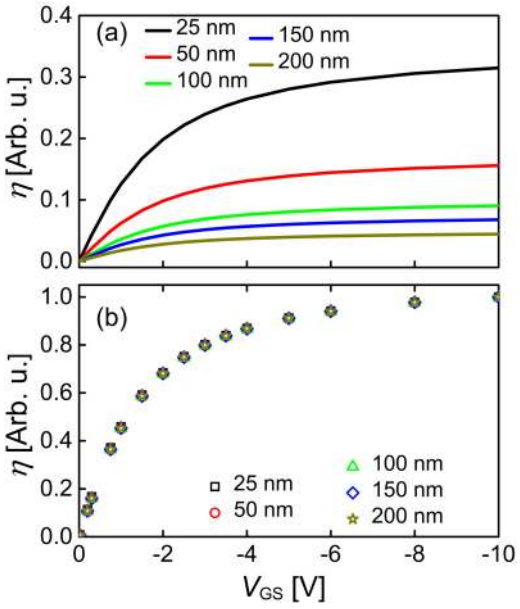

FIG. 7. (a) Relative exciton quenching (η) (in arbitrary units), as a function of V_{GS} for various pentacene thicknesses. (b) η normalized to its value at $V_{GS} = -10$ V.

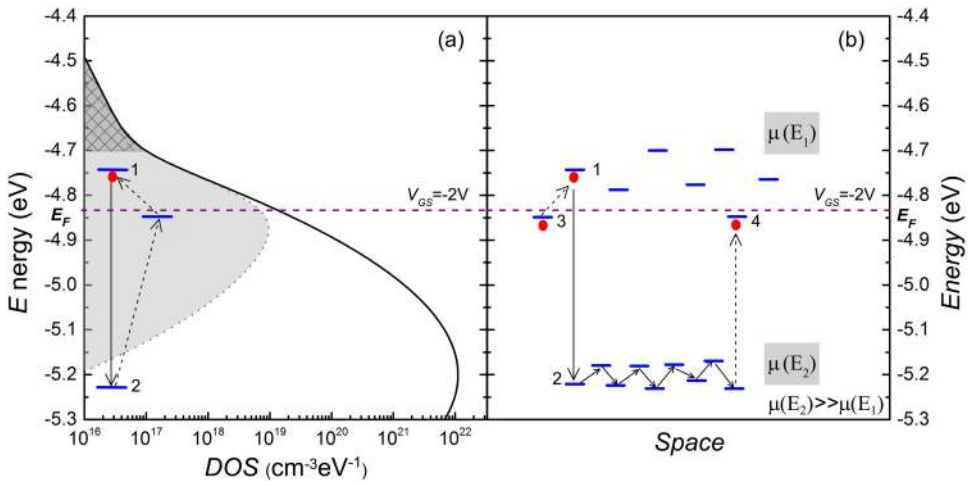

FIG. 8. Polaron activation and thermalization processes leading to photocurrent. (a) A Gaussian density of states (DOS) with a width of 100 meV is assumed. An exponential trap DOS (deep level tail states) with a total density of 10^{17} cm^{-3} (estimated from the subthreshold slope[52]) is added to the primary DOS (deeply shaded area). The lightly shaded area is occupied states at $V_{GS} = -2$ V and for an oxide thickness of 65 nm. E_F is the Fermi level at $V_{GS} = -2$ V. (b) A polaron from state 1 is excited to a higher energy state 2 after receiving the energy from an exciton through the Forster resonant energy transfer (FRET). The excited polaron undergo multiple hopping processes in the higher mobility states. State 1 is then occupied by another polaron from state 3. The polaron excited to state 2 eventually thermalizes to state 4. The multiple hopping processes of the polaron at higher mobility states before its thermalization result in photocurrent.

Fig. 6. At small V_{GS}, the polaron density is low so that all excitons which diffuse to the S/I interface (channel) need not find a polaron to interact with during its lifetime. When V_{GS} increases, the polaron density at the channel increases and the interpolaron separation decreases. This leads to the increase in the number of EPI processes, and hence, more polarons get excited to the high mobility states. At some V_{GS}, the polaron density becomes sufficient enough to quench all the excitons that reach the interface and the number of quenching process saturates. This can explain the saturation of effective n_{PH} at $V_{GS} = -4 \pm 1$ V. The mobility continue increasing with V_{GS} because the polarons can access higher delocalized states.

The absence of the triplet exciton contribution to the photoconduction process was observed in the previous section (Sec. III B). It is known that the triplet binding energy is around half that of the singlet in pentacene.[46] The reduced energy may be insufficient to activate the polaron to a higher energy state in the DOS. Further work is required to understand the low energy triplet interaction with polarons.

The hopping transport ensures sufficient time for the EPI process to occur. In a system with a narrow DOS, bandlike transport can be expected due to the faster hopping rates through the highly delocalized states. In such cases, excitons may not get sufficient time to interact with mobile polarons, which can reduce the exciton loss by EPI.

2. Three-dimensional model for EPI

The contribution of polaron density near the S/I interface to exciton quenching is further confirmed using a simplified model, where the accumulation layer is confined into one monolayer of pentacene at the interface. This is a reasonable assumption, since polaron density reduces by an order of magnitude after one monolayer, as obtained from the TCAD simulation shown in Fig. 2(b) and Fig. S2 in the supplementary material. In this model, the gate-induced polarons reside as a single layer at the S/I interface. A hemispherical volume with a radius $R = L_a$ ($L_a = 10 \pm 2$ nm from Sec. III B) is considered around each polaron in the pentacene layer, termed as the active volume of each polaron. If an exciton is generated within this active volume, it diffuses toward the polaron and quench as shown in the schematic of Fig. 9(a). The relative coordinates of excitons in the volume are located using G_{ex} obtained from the TMM simulation. Relative exciton quenching efficiency (η') is the ratio of the number of excitons that falls within the active volume of polarons to the number of excitons generated in the total volume.

Figure 9(b) shows η' normalized to its value at $V_{GS} = -10$ V for various pentacene thicknesses. A comparison of η' and η (both normalized to the corresponding values at $V_{GS} = -10$ V) is shown in Fig. 9(c), where η' and η follow similar functional dependence with V_{GS}. The V_{GS} corresponding to the knee of saturation of η or n_{PH} ($V_{GS} = -4 \pm 1$ V) can be understood from the saturation of the total active volume, as the hemispheres overlap each other increasingly with decreasing interpolaron distance (d) below $2R$. For an oxide layer with a thickness of 65 nm, $V_{GS} = -4$ V corresponds to a surface charge density of 1.32×10^{12} cm^{-2}. This yields an average separation between two polarons as 8.7 nm, which is in the range of R. This means that saturation of η occurs when the overlapping of active volumes is large enough to cover all the excitons that can diffuse to the interface.

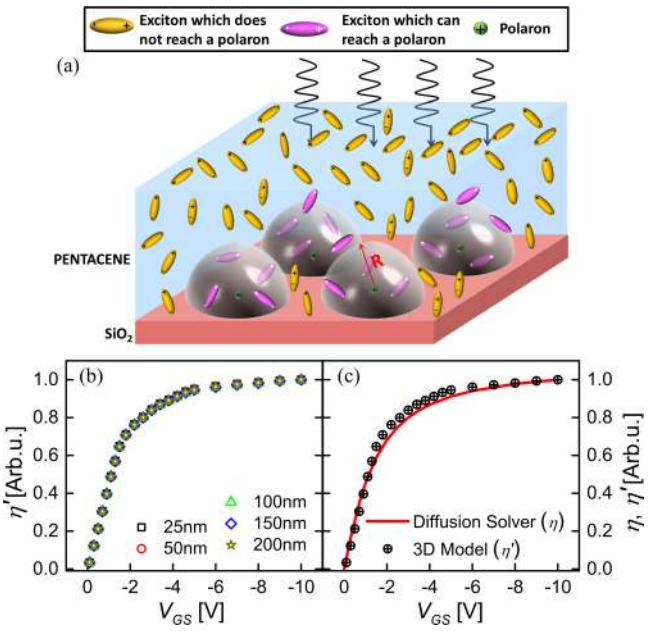

FIG. 9. (a) Schematic of a three-dimensional (3D) model for exciton-polaron interaction. Polarons reside as a single layer at the pentacene/SiO_2 interface, and a hemisphere of radius $R = L_a$ is shown around each polaron. L_a is the active layer thickness obtained from Sec. III B. Excitons generated inside the hemisphere can diffuse toward the polaron and interact. (b) η' (ratio of number of excitons falling within the hemispheres to the number of excitons generated in the total volume), normalized to its value at $V_{GS} = -10$ V and plotted as a function of V_{GS} for different pentacene thicknesses. (c) Comparison of η' and η. η and η' follow the same functional dependence with V_{GS}.

IV. CONCLUSION

In summary, photoconduction in OFETs mediated by the exciton-polaron interaction is studied. The exciton, on quenching after interacting with a polaron, transfers its energy to the polaron. The polaron is promoted to a higher energy state in the density of state manifold and moves in its "hot" state, contributing to the photocurrent. The polycrystalline system with a large density of state width of around 100 meV leads to localized polarons. It is shown that not only the polarons in deep level traps but all polarons interact with excitons. In order to reduce exciton quenching with polarons, a system where the interaction time can be lowered is suggested. This may be possible for systems where the width of the density of states is very low and hence has high levels of delocalization.

SUPPLEMENTARY MATERIAL

See the supplementary material for the additional information mentioned in the paper.

ACKNOWLEDGMENTS

The authors thank the Center for NEMS and Nanophotonics (CNNP) at IIT Madras for facilitating device fabrication and characterization. The authors also thank the reviewers for their useful suggestions which helped shaping the paper in its present form.

REFERENCES

[1]O. Ostroverkhova, "Organic optoelectronic materials: Mechanisms and applications," Chem. Rev. **116**, 13279–13412 (2016).
[2]H.-W. Chen, J.-H. Lee, B.-Y. Lin, S. Chen, and S.-T. Wu, "Liquid crystal display and organic light-emitting diode display: Present status and future perspectives," Light Sci. Appl. **7**, 17168 (2018).
[3]A. J. Kuehne and M. C. Gather, "Organic lasers: Recent developments on materials, device geometries, and fabrication techniques," Chem. Rev. **116**, 12823–12864 (2016).
[4]S. Hirata, Y. Sakai, K. Masui, H. Tanaka, S. Y. Lee, H. Nomura, N. Nakamura, M. Yasumatsu, H. Nakanotani, Q. Zhang, K. Shizu, H. Miyazaki, and C. Adachi, "Highly efficient blue electroluminescence based on thermally activated delayed fluorescence," Nat. Mater. **14**, 330–336 (2015).
[5]H. Kaji, H. Suzuki, T. Fukushima, K. Shizu, K. Suzuki, S. Kubo, T. Komino, H. Oiwa, F. Suzuki, A. Wakamiya, Y. Murata, and C. Adachi, "Purely organic electroluminescent material realizing 100% conversion from electricity to light," Nat. Commun. **6**, 8476 (2015).
[6]T. Miwa, S. Kubo, K. Shizu, T. Komino, C. Adachi, and H. Kaji, "Blue organic light-emitting diodes realizing external quantum efficiency over 25% using thermally activated delayed fluorescence emitters," Sci. Rep. **7**, 284 (2017).
[7]A. S. D. Sandanayaka, T. Matsushima, F. Bencheikh, S. Terakawa, W. J. Potscavage, C. Qin, T. Fujihara, K. Goushi, J.-C. Ribierre, and C. Adachi, "Indication of current-injection lasing from an organic semiconductor," Appl. Phys. Exp. **12**, 061010 (2019).
[8]I. D. W. Samuel and G. A. Turnbull, "Organic semiconductor lasers," Chem. Rev. **107**, 1272–1295 (2007).
[9]S. Zulkarnaen Bisri, T. Takenobub, and Y. Iwasacd, "The pursuit of electrically-driven organic semiconductor lasers," J. Mater. Chem. C **2**, 2827–2836 (2014).
[10]M. Deussen, M. Scheidler, and H. Bässler, "Electric field-induced photoluminescence quenching in thin-film light-emitting diodes based on poly (phenyl-p-phenylene vinylene)," Synth. Met. **73**, 123–129 (1995).
[11]S. Haneder, E. Da Como, J. Feldmann, M. M. Rothmann, P. Strohriegl, C. Lennartz, O. Molt, I. Münster, C. Schildknecht, and G. Wagenblast, "Effect of electric field on Coulomb-stabilized excitons in host/guest systems for deep-blue electrophosphorescence," Adv. Funct. Mater. **19**, 2416–2422 (2009).
[12]J. Kalinowski, W. Stampor, and J. Szmytkowski, "Coexistence of dissociation and annihilation of excitons on charge carriers in organic phosphorescent emitters," Phys. Rev. B **74**, 085316 (2006).
[13]V.-E. Choong, Y. Park, Y. Gao, B. R. Hsieh, and C. W. Tang, "Metal induced photoluminescence quenching of a phenylene vinylene oligomer and its recovery," Macromol. Symp. **125**, 83–97 (1998).
[14]A. L. Burin and M. A. Ratner, "Exciton migration and cathode quenching in organic light emitting diodes," J. Phys. Chem. A **104**, 4704–4710 (2000).
[15]M. A. Baldo, C. Adachi, and S. R. Forrest, "Transient analysis of organic electrophosphorescence. II. Transient analysis of triplet-triplet annihilation," Phys. Rev. B **62**, 10967–10977 (2000).
[16]A. Ruseckas, J. C. Ribierre, P. E. Shaw, S. V. Staton, P. L. Burn, and I. D. W. Samuel, "Singlet energy transfer and singlet-singlet annihilation in light-emitting blends of organic semiconductors," Appl. Phys. Lett. **95**, 183305 (2009).
[17]Y. Zhang, M. Whited, M. E. Thompson, and S. R. Forrest, "Singlet–triplet quenching in high intensity fluorescent organic light emitting diodes," Chem. Phys. Lett. **495**, 161–165 (2010).
[18]M. Lehnhardt, T. Riedl, T. Weimann, and W. Kowalsky, "Impact of triplet absorption and triplet-singlet annihilation on the dynamics of optically pumped organic solid-state lasers," Phys. Rev. B **81**, 165206 (2010).
[19]W. Helfrich, "Destruction of triplet excitons in anthracene by injected electrons," Phys. Rev. Lett. **16**, 401–403 (1966).
[20]V. Ern, H. Bouchriha, J. Fourny, and G. Delacôte, "Triplet exciton-trapped hole interaction in anthracene crystals," Solid State Commun. **9**, 1201–1203 (1971).

[21]R. Karpicz, M. Kirkus, J. Vidas Grazulevicius, and V. Gulbinas, "Fluorescence quenching by charge carriers in indolo[3,2-b]carbazole-based polymer," J. Lumin. **130**, 722–727 (2010).
[22]J. C. Bolinger, M. C. Traub, T. Adachi, and P. F. Barbara, "Ultralong-range polaron-induced quenching of excitons in isolated conjugated polymers," Science **331**, 565–567 (2011).
[23]J. M. Hodgkiss, S. Albert-Seifried, A. Rao, A. J. Barker, A. R. Campbell, R. A. Marsh, and R. H. Friend, "Exciton-charge annihilation in organic semiconductor films," Adv. Funct. Mater. **22**, 1567–1577 (2012).
[24]W. A. Koopman, M. Natali, G. P. Donati, M. Muccini, and S. Toffanin, "Charge exciton interaction rate in organic field-effect transistors by means of transient photoluminescence electromodulated spectroscopy," ACS Photonics **4**, 282–291 (2017).
[25]R. Capelli, S. Toffanin, G. Generali, H. Usta, A. Facchetti, and M. Muccini, "Organic light-emitting transistors with an efficiency that outperforms the equivalent light-emitting diodes," Nat. Mater. **9**, 496–503 (2010).
[26]N. H. Hansen, C. Wunderlich, A. K. Topczak, E. Rohwer, H. Schwoerer, and J. Pflaum, "Exciton interaction with a spatially defined charge accumulation layer in the organic semiconductor diindenoperylene," Phys. Rev. B **87**, 241202 (2013).
[27]B. Verreet, A. Bhoolokam, A. Brigeman, R. Dhanker, D. Cheyns, P. Heremans, A. Stesmans, N. C. Giebink, and B. P. Rand, "Reducing exciton-polaron annihilation in organic planar heterojunction solar cells," Phys. Rev. B **90**, 115304 (2014).
[28]A. S. D. Sandanayaka, K. Yoshida, T. Matsushima, and C. Adachi, "Exciton quenching behavior of thermally activated delayed fluorescence molecules by charge carriers," J. Phys. Chem. C **119**, 7631–7636 (2015).
[29]F. Montilla, A. Ruseckas, and I. D. W. Samuel, "Exciton-polaron interactions in polyfluorene films with β-phase," J. Phys. Chem. C **122**, 9766–9772 (2018).
[30]W. W. A. Koopman, S. Toffanin, M. Natali, S. Troisi, R. Capelli, V. Biondo, A. Stefani, and M. Muccini, "Mapping of charge distribution in organic field-effect transistors by confocal photoluminescence electromodulation microscopy," Nano Lett. **14**, 1695–1700 (2014).
[31]H. S. Tan, N. Mathews, T. Cahyadi, F. R. Zhu, and S. G. Mhaisalkar, "The effect of dielectric constant on device mobilities of high-performance, flexible organic field effect transistors," Appl. Phys. Lett. **94**, 263303 (2009).
[32]C. Y. Wei, S. H. Kuo, Y. M. Hung, W. C. Huang, F. Adriyanto, and Y. H. Wang, "High-mobility pentacene-based thin-film transistors with a solution-processed barium titanate insulator," IEEE Electron Device Lett. **32**, 90–92 (2011).
[33]C. C. Shen, W. Y. Chou, and H. L. Liu, "Temperature dependence of optical properties of pentacene thin films probed by spectroscopic ellipsometry," Solid State Commun. **188**, 1–4 (2014).
[34]M. Yi, J. Guo, W. Li, L. Xie, Q. Fan, and W. Huang, "High-mobility flexible pentacene-based organic field-effect transistors with PMMA/PVP double gate insulator layers and the investigation on their mechanical flexibility and thermal stability," RSC Adv. **5**, 95273–95279 (2015).
[35]W. F. Pasveer, J. Cottaar, C. Tanase, R. Coehoorn, P. A. Bobbert, P. W. Blom, M. De Leeuw, and M. A. Michels, "Unified description of charge-carrier mobilities in disordered semiconducting polymers," Phys. Rev. Lett. **94**, 206601 (2005).
[36]S. Yogev, E. Halpern, R. Matsubara, M. Nakamura, and Y. Rosenwaks, "Direct measurement of density of states in pentacene thin film transistors," Phys. Rev. B **84**, 165124 (2011).
[37]Synopsys,"Sentaurus TCAD Release H-2013.03," Mountain View, CA, USA.
[38]V. Arkhipov, E. Emelianova, and H. Bässler, "Hot exciton dissociation in a conjugated polymer," Phys. Rev. Lett. **82**, 1321–1324 (1999).
[39]V. Arkhipov, E. Emelianova, S. Barth, and H. Bässler, "Ultrafast on-chain dissociation of hot excitons in conjugated polymers," Phys. Rev. B **61**, 8207–8214 (2000).
[40]J. Lloyd-Hughes, T. Richards, H. Sirringhaus, M. B. Johnston, and L. M. Herz, "Exciton dissociation in polymer field-effect transistors studied using terahertz spectroscopy F8T2," Phys. Rev. B **77**, 125203 (2008).
[41]K. Ohta and H. Ishida, "Matrix formalism for calculation of electric field intensity of light in stratified multilayered films," Appl. Opt. **29**, 1952–1959 (1990).
[42]S. Gorgolis, A. Giannopoulou, D. Anastassopoulos, and P. Kounavis, "Impact of pentacene film thickness on the photoresponse spectra: Determination of the photocarrier generation mechanism," J. Appl. Phys. **112**, 013101 (2012).
[43]D. Ray, M. Furno, E. Siebert-Henze, K. Leo, and M. Riede, "Quantitative estimation of electronic quality of zinc phthalocyanine thin films," Phys. Rev. B **84**, 075214 (2011).
[44]A. J. Ferguson, N. Kopidakis, S. E. Shaheen, and G. Rumbles, "Quenching of excitons by holes in poly (3-hexylthiophene) films," J. Phys. Chem. C **112**, 9865–9871 (2008).
[45]D. N. Congreve, J. Lee, N. J. Thompson, E. Hontz, S. R. Yost, P. D. Reusswig, M. E. Bahlke, S. Reineke, T. V. Voorhis, and M. A. Baldo, "External quantum efficiency above 100% in a singlet-exciton-fission-based organic photovoltaic cell," Science **340**, 334–337 (2013).
[46]M. W. B. Wilson, A. Rao, J. Clark, R. S. S. Kumar, D. Brida, G. Cerullo, and R. H. Friend, "Ultrafast dynamics of exciton fission in polycrystalline pentacene," J. Am. Chem. Soc. **133**, 11830–11833 (2011),
[47]A. D. Poletayev, J. Clark, M. W. Wilson, A. Rao, Y. Makino, S. Hotta, and R. H. Friend, "Triplet dynamics in pentacene crystals: Applications to fission-sensitized photovoltaics," Adv. Mater. **26**, 919–924 (2014).
[48]S. Yoo, W. J. Potscavage, B. Domercq, S. H. Han, T. D. Li, S. C. Jones, R. Szoszkiewicz, D. Levi, E. Riedo, S. R. Marder, and B. Kippelen, "Analysis of improved photovoltaic properties of pentacene/C60 organic solar cells: Effects of exciton blocking layer thickness and thermal annealing," Solid-State Electron. **51**, 1367–1375 (2007).
[49]H. Marciniak, I. Pugliesi, B. Nickel, and S. Lochbrunner, "Ultrafast singlet and triplet dynamics in microcrystalline pentacene films," Phys. Rev. B Condens. Matter Mater. Phys. **79**, 235318 (2009).
[50]M. C. J. M. Vissenberg and M. Matters, "Theory of the field-effect mobility in amorphous organic transistors," Phys. Rev. B **57**, 12964–12967 (1998).
[51]C. Tanase, E. J. Meijer, P. W. Blom, and D. M. de Leeuw, "Unification of the hole transport in polymeric field-effect transistors and light-emitting diodes," Phys. Rev. Lett. **91**, 216601 (2003).
[52]W. L. Kalb and B. Batlogg, "Calculating the trap density of states in organic field-effect transistors from experiment: A comparison of different methods," Phys. Rev. B Condens. Matter Mater. Phys. **81**, 035327 (2010).
[53]Z. Jia, L. Banu, and I. Kymissis, "Photocurrent study of oxygen-mediated doping states in pentacene thin-film transistors," IEEE Trans. Electron Devices **57**, 380–384 (2010).
[54]L. Onsager, "Initial recombination of ions," Phys. Rev. **54**, 554–557 (1938).
[55]V. I. Arkhipov and H. Bässler, "Exciton dissociation and charge photogeneration in pristine and doped conjugated polymers," Phys. Status Solidi (A) Appl. Res. **201**, 1152–1187 (2004).
[56]M. Pope and H. Swenberg, *Electronic Processes in Organic Crystals and Polymers*, 2nd ed. (Oxford University Press, New York, 1999), pp. 164–166.
[57]J. Reynaert, V. I. Arkhipov, P. Heremans, and J. Poortmans, "Photomultiplication in disordered unipolar organic materials," Adv. Funct. Mater. **16**, 784–790 (2006).
[58]S. M. Menke, A. Cheminal, P. Conaghan, N. A. Ran, N. C. Greehnam, G. C. Bazan, T.-Q. Nguyen, A. Rao, and R. H. Friend, "Order enables efficient electron-hole separation at an organic heterojunction with a small energy loss," Nat. Commun. **9**, 277 (2018).
[59]J. Y. Lee, S. Roth, and Y. W. Park, "Anisotropic field effect mobility in single crystal pentacene," Appl. Phys. Lett. **88**, 252106 (2006).
[60]M. H. Cohen, E. N. Economou, and C. M. Soukoulis, "Microscopic mobility," Phys. Rev. B **30**, 4493–4500 (1984).